JACS Au
AN OPEN ACCESS JOURNAL OF THE AMERICAN CHEMICAL SOCIETY

pubs.acs.org/jacsau
Article

Atomic Layer Deposition of the Geometry Separated Lewis and Brønsted Acid Sites for Cascade Glucose Conversion

Wenjie Yang, Xiao Liu, Luke A. O'Dell, Xingxu Liu, Lizhuo Wang, Wenwen Zhang, Bin Shan, Yijiao Jiang, Rong Chen,* and Jun Huang*

Cite This: JACS Au 2023, 3, 2586−2596
Read Online
ACCESS | Metrics & More | Article Recommendations | Supporting Information

ABSTRACT: Solid acid catalysts with bi-acidity are promising as workhouse catalysts in biorefining to produce high-quality chemicals and fuels. Herein, we report a new strategy to develop bi-acidic cascade catalysts by separating both acid sites in geometry via the atomic layer deposition (ALD) of Lewis acidic alumina on Brønsted acidic supports. Visualized by transmission electron microscopy and electron energy loss spectroscopy mapping, the ALD-deposited alumina forms a conformal alumina domain with a thickness of around 3 nm on the outermost surface of mesoporous silica−alumina. Solid state nuclear magnetic resonance investigation shows that the dominant Lewis acid sites distribute on the outermost surface, whereas intrinsic Brønsted acid sites locate inside the nanopores within the silica-rich substrate. In comparison to other bi-acidic solid catalyst counterparts, the special geometric distance of Lewis and Brønsted acid sites minimized the synergetic effect, leading to a cascade reaction environment. For cascade glucose conversion, the designed ALD catalyst showed a highly enhanced catalytic performance.

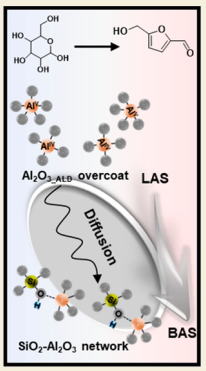

KEYWORDS: *Bi-acidic catalyst, Atomic layer deposition, Brønsted acid site, Lewis acid site, Cascade reaction*

INTRODUCTION

Solid acid, as the most popular heterogeneous catalyst, has received much research and industrial interest in promoting sustainable hydrocarbon transformation and biorefining. Among solid acids, due to the advantages of tunable surface acidity of both Lewis acid site (LAS) and Brønsted acid site (BAS), large specific surface area, adjustable porosity, and cheap synthesis, aluminosilicate materials attracted the most attention.[1−3] Generally, on crystalline aluminosilicates, such as zeolites, the penetration of four-coordinated aluminum species into the tetrahedral silica framework contributes to the establishment of BAS via the formation of bridging hydroxyl structure for compensating local negative charges,[4] whereas the dihydroxylation, steaming, or dealumination resulting in extra-framework Al species on zeolites are believed to be the origin of surface Lewis acidity.[5] Therefore, both BAS and LAS on zeolites contribute to the bi-acidic catalysts, where a synergistic effect between Brønsted-Lewis pairs has been observed.[6,7] The synergistic effect gives enhancement of Brønsted acidity for the catalysis,[8,9] and the cooperation between both acid sites leads to the enhanced performance of multistep catalytic conversion.[10,11]

However, the spatially adjacent BAS-LAS pairs on zeolites generally contribute to the ultrastrong acidity of BAS via LAS withdrawing electron pair from the BAS hydroxyl group. This is beneficial only for catalytic reactions that require strong acidity. For example, with a spatial interaction between a Lewis acidic Zn^{2+} cation and Brønsted acidic SiOHAl, the synergetic effect contributes to an ultrastrong BAS that enhances the activation of the methane C−H bond.[12] The Ga^{3+}-BAS pair results in the enhanced acid strength of Ga-modified ZSM-5, which contributes to an enhanced aromatic selectivity on methanol-to-aromatic conversion.[13] Caused by the polarizing effect of multivalent extra-framework Al cations on the SiOHAl group of BAS, the BAS shows a much stronger interaction with the basic probe molecule of acetonitrile (CD_3CN) compared to that of zeolite H, Na−X and H, Na−Y.[14] Nevertheless, the ultrastrong acid site limits the cascade reaction on both sites and results in lower selectivity for the target products due to side reactions such as overoxidation.[3,15,16] Additionally, the microporous nature of zeolites restricts the entry and diffusion of bulky biomass molecules, limiting their access to the active sites, which further hurdles performance.[17]

In this research, we develop the synthesis strategy to separate BAS and LAS in geometry and promote the cascade reactions on both acid sites via atomic layer deposition (ALD) of the LAS-based domain on BAS-based supports. ALD, as a method to grow thin films, has been considered as a way to coat uniform conformal overlayers and tune the surface

Received: July 20, 2023
Revised: August 20, 2023
Accepted: August 22, 2023
Published: September 6, 2023

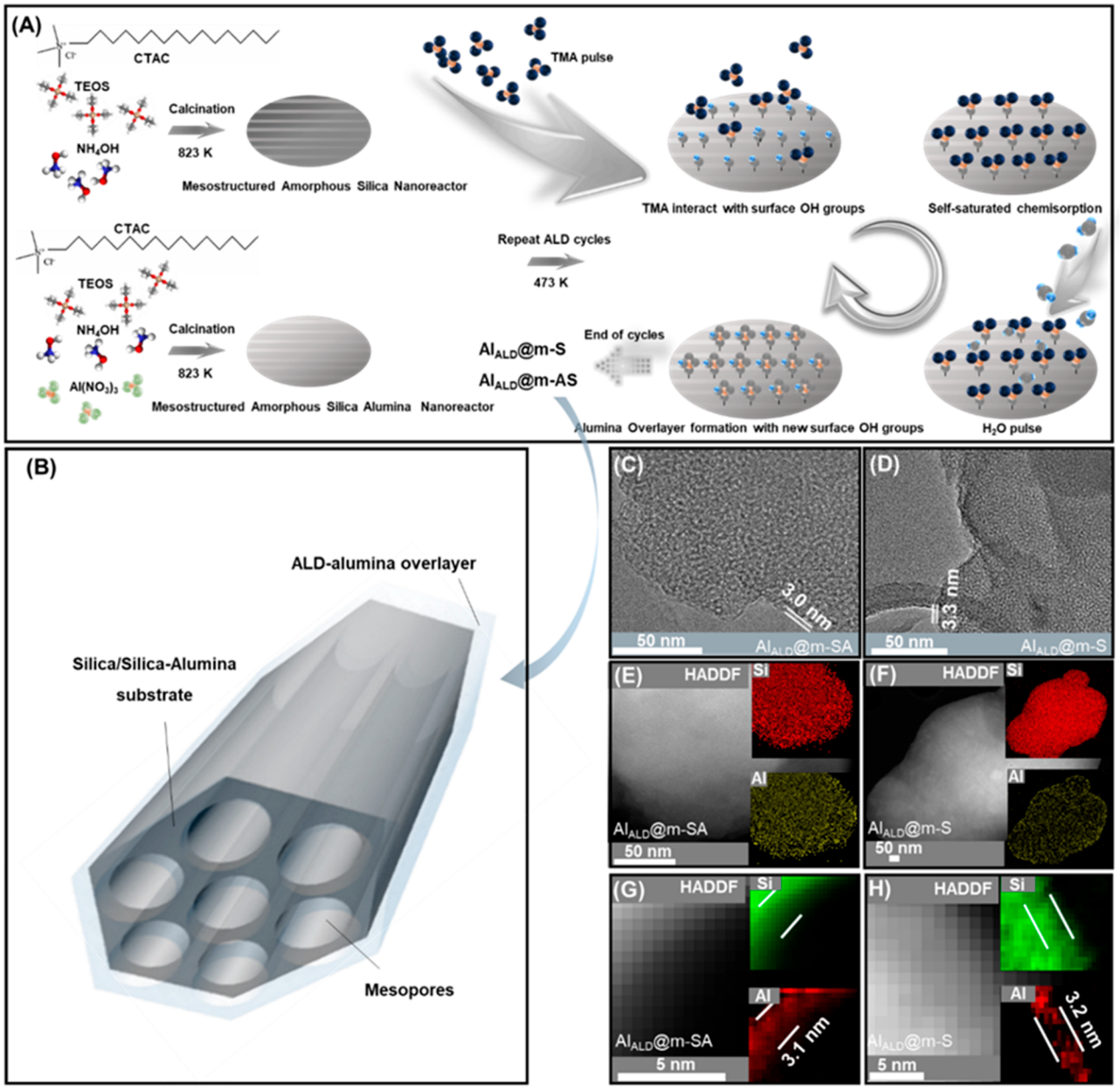

Figure 1. (A) Scheme of Al_{ALD}@high silica substrate synthetic approach; (B) Schematic diagram of Al_{ALD}/high silica substrate; HRTEM images of (C) Al_{ALD}/m-SA and (D) Al_{ALD}/m-S; EDS mapping image of (E) Al_{ALD}/m-SA and (F) Al_{ALD}/m-S; electron energy loss EDS-Mappings of (G) Al_{ALD}/m-SA and (H) Al_{ALD}/m-S.

properties of catalysts within defined overlayer regions.[18] Currently, ALD has been mainly applied in BAS formation and the improvement of silica−alumina catalysts. Stair et al.[19] observed the BAS formation ability of the ALD-deposited nonacidic SiO_2 overlayer on alumina. The formed BAS-based $(AlO)_3Si(OH)$ sites showed an enhanced catalytic performance on cyclohexanol dehydration. Ardagh et al.[20] demonstrated the criticalness of the thickness of the overcoat layer to the formation of BAS on the external surface. They found that the catalyst with ∼2 nm coatings of SiO_x on Al_2O_3 substrate gives the highest BAS concentration, and the prepared BAS on the external surface leads to enhanced performance on 1,3,5-triisopropylbenzene cracking. Similarly, coating alumina on silica also contributes to BAS. Krishna et al.[21] identified the formation of surface BAS between the ALD-formed alumina overlayer and the silica substrate. With 5−10 ALD cycles, the majority of isolated SiOH can be covered, contributing to an enhanced concentration of BAS. Nevertheless, little research focuses on the formation and development of LAS via ALD on silica−alumina catalysts.

Herein, via atomic layer deposited alumina, we develop an LAS-based domain on the external surface of a BAS-based mesoporous silica−alumina substrate and hide the majority of the intrinsic BAS of the substrate inside the nanopores. Thus, BAS and LAS have been separated by the geometry in the catalysts, which is promising for cascade reactions with controlled diffusion. The geometry of the prepared catalysts and the distribution of ALD alumina are characterized by high-resolution transmission electron microscopy (HRTEM) combined with electron energy loss spectroscopy (EELS) mapping. Multinuclear ssNMR was used to characterize the BAS and LAS of the samples. Among biomass conversions with

https://doi.org/10.1021/jacsau.3c00396
JACS Au 2023, 3, 2586−2596

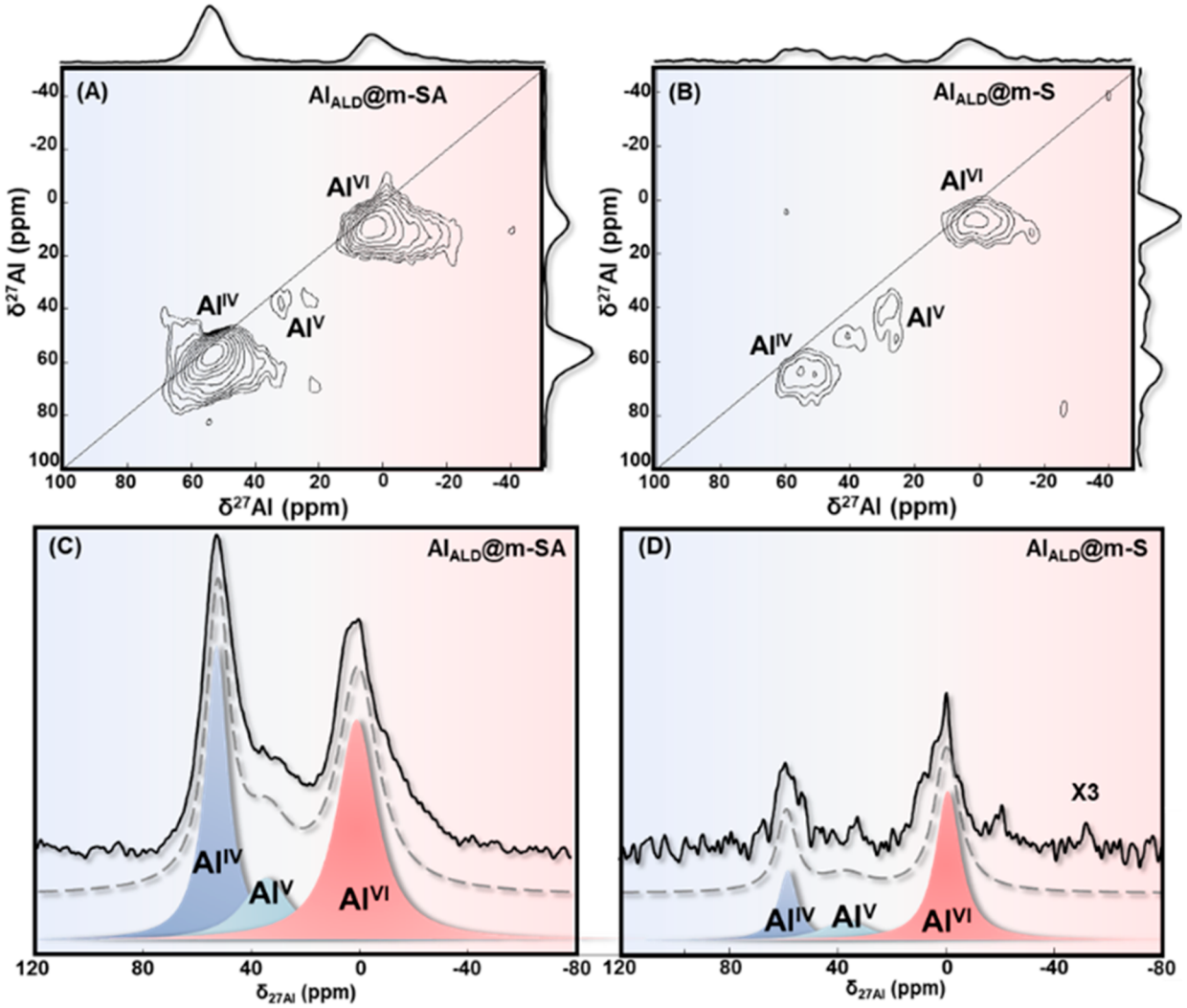

Figure 2. Sheared 2D ^{27}Al MQMAS NMR spectra of (A) Al_{ALD}@m-SA and (B) Al_{ALD}@m-S. Contours between F1 and F2 dimensions have been assigned to aluminum species based on the isotropic chemical shift. (C) and (D) 1D ^{27}Al MAS NMR spectra and the corresponding simulations (X3 refers to that the signal has been magnified three times).

complex reaction networks,[22−24] converting glucose into platform chemicals 5-hydroxymethylfurfural (HMF) stands as one of the most promising routes for green chemistry.[2,25] Thus, the typical biorefining cascade glucose conversion is applied as the testing reaction for the cascade performance of the prepared catalysts.

RESULTS AND DISCUSSION

Synthesis and Geometry of ALD Catalysts

To construct the precisely controlled cascade architectural structure, the ALD cycles under elevated temperature were conducted in order to make nanolevel architectural modification on the outermost surface. The TMA pulses led to the formation of the Al−C bonds on the outermost surface of the substrate via the replacement of surface silanol hydroxyl protons with Al ions, which provides the prerequisites of the formation of the unique geometry of alumina nanolayer on the silica-based substrates.[26] The following H_2O pulse contributed to the replacement of the outermost surface Al−C bonds with Al−O bonds and led to the formation of alumina nanofilm. With more ALD cycles, the protons of surface AlOH groups can continue to be replaced by Al ions, leading to the increase in the thickness of the alumina nanolayer (Figure 1A,B).

The geometry of the ALD silica−alumina catalysts has been visualized by high-resolution transmission electron microscopy (HRTEM). As shown in Figure 1C,D, on the outermost surface of the prepared catalysts, a thin nanolayer with similar thickness (d = 3.0 nm and d = 3.3 nm, respectively) can be observed. This finding is in line with the observation of a translucent covering layer in HRTEM images for Al_2O_{3ALD}-SiO_2,[27] SiO_{2MLD}-TiO_2,[28] and Al_{ALD}-Pt/Al_2O_3.[29] It supports that the ALD process predominantly creates an alumina nanolayer on the outermost surface as an overcoat instead of dispersing aluminum species into the nanopores or network lattice of the support, which is independent of the substrate composition. Compared to the parent substrates, this is consistent with the observed the small reduction in surface area and pore volume characterized via nitrogen adsorption/desorption (Figures S1 and S3, Tables S1−2), where the ALD-alumina overcoat geometrically partially fill or cap the mesopores. Besides, the absence of crystalline structure in HRTEM images agrees well with the X-ray amorphous structure (Figure S2), demonstrating that not only the

https://doi.org/10.1021/jacsau.3c00396
JACS Au 2023, 3, 2586−2596

amorphous nature of the material remained after ALD treatment, but also the alumina overcoat from ALD deposition maintained an amorphous geometry. The EDS elemental mappings in Figure 1E,F demonstrate the shell-like homogeneous coverage of alumina thin overcoat on the support. The absence of an obvious isolated Al domain could contribute to the rapid surface Al−O−Al condensation,[30] hinting that no large aggregation of alumina had been formed during the ALD aluminum deposition. Furthermore, to visualize the detailed nanolevel local geometry of the prepared cascade architectural silica−alumina, the electron energy loss (EELS) EDS mapping has been applied. In the Figure 1G,H, the ALD deposited alumina geometrically contributes to a nanolevel shell with *ca.* 3 nm thickness. Table S2 summarizes the physicochemical properties of Al_{ALD}@high silica substrate samples. Based on the surface composition characterization via XPS surface elemental analysis, the surface $n(Si)/n(Al)_{surface}$ of the Al_{ALD}@high silica substrate is much smaller compared to that of the parent substrates (Tables S1−2). This finding also supports the visualized observation of the outermost surface distribution of alumina.

Thus, with the characterization evidence mentioned above, regardless of the substrate, we demonstrated that the ALD process can generate a shell-like thin alumina nanolayer with *ca.* 3 nm in thickness (0.15 nm/cycle) on the substrate while having minimal effect on the existing global geometry (Figure 1B).

Acidity Characterization of ALD Catalysts

The characterization of acid sites and their local structure was performed by multinuclear solid-state NMR spectroscopy. With the ability of spin manipulation to avoid second-order quadripolar line broadening, 2D ^{27}Al MQMAS NMR has been conducted (Figure 2A,B) for resolving Al coordination of ALD catalysts with higher resolution and which can be utilized to predict the surface acidity.[31] The isotropic chemical shift demonstrated the presence of four-coordinated Al (Al^{IV}, δ_{iso} = *ca.* 57 ppm), five-coordinated Al (Al^{V}, δ_{iso} = *ca.* 36 ppm), and six-coordinated Al (Al^{VI}, δ_{iso}= *ca.* 7 ppm) in the samples. With the ALD of alumina on pure silica support (Al_{ALD}@m-S), the 2D ^{27}Al MQMAS NMR spectrum and the corresponding 1D ^{27}Al MAS NMR spectrum of Al_{ALD}@m-S are similar to that of the pure Al_2O_3[32] (Figure 2B,D). With the fitting on 1D ^{27}Al MAS NMR spectra for quantitative evaluation of Al species, the Al_{ALD}@m-S showed a dominant Al^{VI} species (70.9%, Table 1), which was generally the contributor of the surface LAS.[33]

Table 1. Summary of Deconvolution Results and DMFit Calculated Aluminum Species Molar Ratio

catalyst	Al^{IV} (%)	Al^{V} (%)	Al^{VI} (%)
Al_{ALD}@m-SA	36.2	18.3	45.5
Al_{ALD}@m-S	21.3	7.8	70.9
m-SA[25]	94.0	-	6.0

Differently, the 2D ^{27}Al MQMAS NMR spectrum recorded both strong Al^{VI} and Al^{IV} signals of ALD-alumina on mesoporous silica−alumina (Al_{ALD}@m-SA) (Figure 2A), and the corresponding 1D ^{27}Al MAS NMR spectrum showed a relatively balanced Al^{VI} and Al^{IV} ratio (36.2% and 45.5% for Al^{IV} and Al^{VI}, respectively; Figure 2C). Similar to Al_{ALD}@m-S, the surface exposed Al^{VI} species on the ALD deposited alumina nanolayer can generate LAS on external surface of m-SA, while the Al^{IV} species inside the silica network on nanopores of the m-SA support led to the presence of BAS.[24]

With the help of the TMPO probe molecule, ^{31}P MAS NMR has been utilized to quantitatively test the LAS and BAS acidity on ALD catalysts. Numerous studies demonstrated that TMPO can perform as a functional molecular probe for characterizing the type, strength, and accessibility of surface acid sites.[34−36] With accessible BAS inside nanopores, a hydrogen bond can be formed between the hydroxyl proton of BAS and the oxygen atoms of P═O, giving δ_{31P} = 65 to 67 ppm in ^{31}P MAS NMR spectra (Figure 3).[37] The direct adsorption of TMPO on LAS also contributes to δ_{31P} = 43−45 ppm in the ^{31}P MAS NMR spectra (Figure 3). This is attributed to the positive charge compensation of LAS by the electron cloud density around the ^{31}P nucleus. The chemical shifts observed in the ^{31}P MAS NMR spectra of the TMPO-loaded samples are indicative of the acidic strength of the acid sites within the catalyst. The chemical shifts observed suggest that this catalyst exhibits moderate acidity.[37]

The one-dimensional ^{31}P MAS NMR spectra provide quantitative information on the surface-accessible acid sites (Figure 3A−C). With the predominant Al^{IV} species on the m-SA substrate, the m-SA support exhibits a predominant Brønsted acidity of 0.17 μmol/g (Figure 3A, Table S1). With the identified strong Al^{VI} signal intensity, the Al_{ALD}@m-S had a dominant surface LAS of 0.19 μmol/g (Figure 3B, Table S2). Because the network with pure silica (m-S) exhibits almost no acidity, this observation confirmed that the ALD process produces mainly LAS on the outermost surface of mesoporous silica. The generated 0.01 μmol/g BAS could contribute to the BAS at the interface between the silica domain of the m-S substrate and the ALD-produced alumina nanolayer domain. In Al_{ALD}@m-SA, the BAS has a ten times higher concentration (0.10 μmol/g) compared to that of Al_{ALD}@m-S. It can be explained by the BAS originally existing on the mesopores of the m-SA support, which was not overlapped by the surface LAS generated by the ALD process and was still accessible to the reactant (Figure 3C). This is in agreement with the predominance of BAS on m-SA (Figure 3A). Besides, the lower BAS concentration in Al_{ALD}@m-SA compared to that of m-SA confirmed that the ALD generated alumina overlayer covered the majority of the BAS on the external surface of the m-SA substrate but leaves BAS on nanopores intact (0.17 and 0.10 μmol/g for m-SA and Al_{ALD}@m-SA, respectively, Tables S1−2). Additionally, the similar LAS concentrations observed on both catalysts (0.19 and 0.22 μmol/g for Al_{ALD}/m-S and Al_{ALD}/m-SA, respectively, Table S2) confirm that the identical ALD deposition contributes to the surface LAS on the outermost alumina nanolayer and which is spatially and chemically independent with the BAS inside the nanopores. Thus, the spatially separated acid site distribution is drawn in Figure 3D, where BAS is located inside the nanopores and LAS on the external surface.

Cascade Glucose Conversion on ALD Catalysts

The glucose conversion to HMF is a widely studied biomass value-added cascade reaction driven by bi-acidic catalysts and the selectivity of which is largely determined by the acidic properties of the catalyst.[38] It is widely accepted that the LAS promotes the isomerization of glucose to fructose, while BAS is responsible for the secondary dehydration step.[39,40] For the applied catalysts, with predominant accessible nonacidic SiOH, accessible surface BAS, and predominant surface LAS on m-S,

https://doi.org/10.1021/jacsau.3c00396
JACS Au 2023, 3, 2586−2596

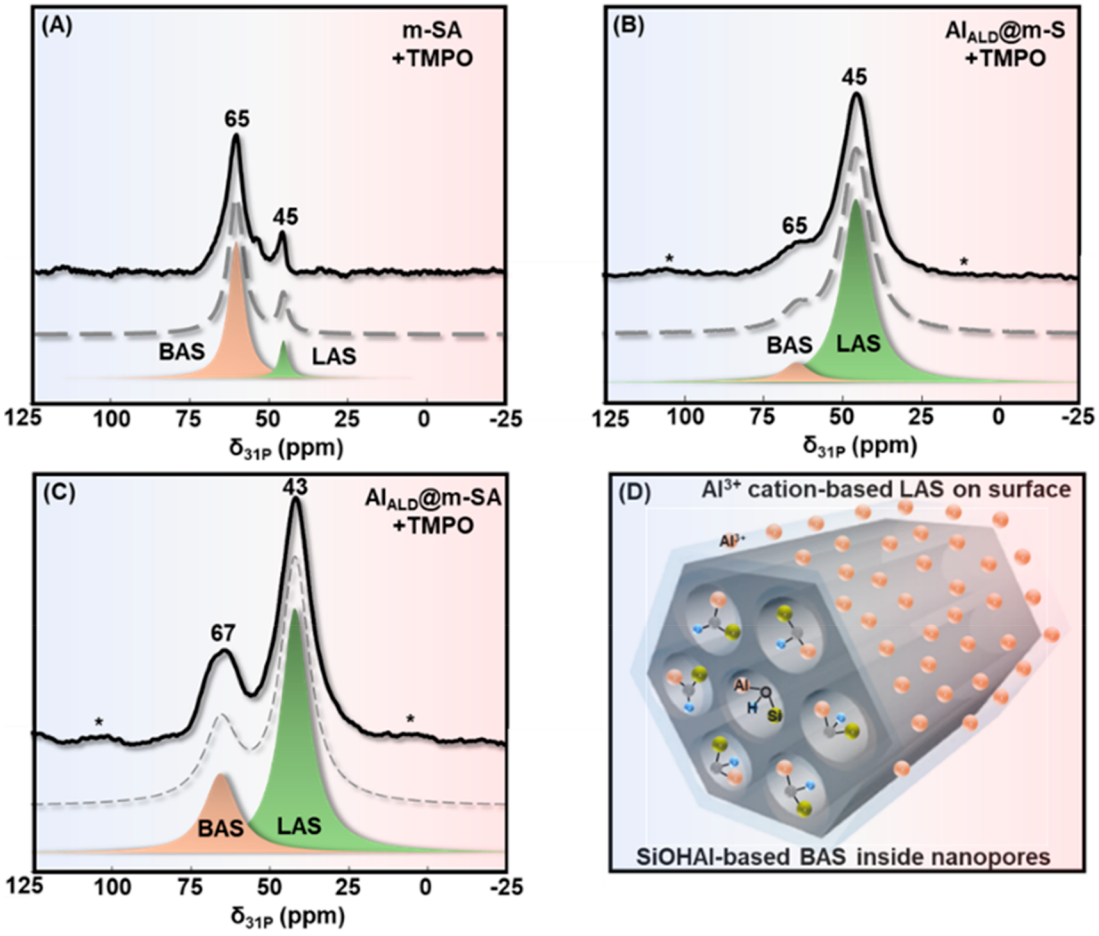

Figure 3. ^{31}P MAS NMR spectra of (A)m-SA, (B)Al_{ALD}@m-S, and (C) Al_{ALD}@m-SA catalysts (*represent sidebands) (black line: spectra, dashed line: simulations; colored blocks: components), (D) the proposed schemetic diagram of the acid site distrubution on Al_{ALD}@m-SA.

m-SA, and Al_{ALD}@m-S surface, these catalysts are assigned to be catalysts with nonacidity, predominant Brønsted acidity, and predominant Lewis acidity, respectively. The Al_{ALD}@m-SA catalyst with LAS on the external surface and BAS inside the nanopores is assigned to the cascade-structured bi-acidic catalyst, as characterized above.

As shown in Figure S6, with the absence of an acid site (m-S), only low conversion ($C_{Glucose,\ 180\ min}$ = 21%) can be identified. The reaction rate constants could not be optimized from the nonlinear least-squares regression (not shown). Moderate conversions of glucose can be observed on catalysts with either predominant Lewis acidity (Al_{ALD}@m-S, Figure 4A) or Brønsted acidity (m-SA, Figure 4B). With dominant surface Lewis acidity on the ALD deposited alumina overlayer of Al_{ALD}@m-S, the constant rates of glucose decomposition is doubled compared to nonacidic m-S (k_G = 0.00309 and 0.00154 min^{-1}, respectively, Table S4). This suggests the importance of LAS in glucose activation, and this is also consistent with the observed relationship between chemical hardness and experimental HMF yields in the rate-limiting step of glucose-to-fructose isomerization for six metal chlorides.[41]

With only a few accessible BAS on the interface of the outermost alumina nanolayer and pure silica substrate, the selectivity of HMF did not increase obviously with the increase in reaction time ($S_{HMF,60\ min}$ = 13% vs $S_{HMF,180\ min}$ = 17%, respectively, Table 2). The accumulation of intermediate fructose with the evolution of time ($S_{fructose,180\ min}$ = 20%) on the Al_{ALD}@m-S agreed well with the reported claim that the LAS contributes little to the dehydration of fructose but only to the glucose isomerization. Consistently, regarding fructose dehydration, the observed low conversion rate and HMF selectivity on Al_{ALD}@m-S ($C_{Fructose,\ 90\ min}$ = 40% and $S_{HMF,90\ min}$ = 13%, Figure 4D) proved that the predominant LAS contribute little to the dehydration of fructose to HMF.

With predominant BAS, the m-SA catalyst showed enhanced glucose conversion and HMF selectivity, where HMF selectively achieved a maximum of $S_{HMF,180\ min}$ = 39% (Figure 4B). The enhanced glucose conversion on BAS catalyst compared to LAS catalyst could be explained by the easier glucose isomerization compared to fructose dehydration at elevated temperature without acid sites; the former can occur faster with a smaller energy barrier.[42] The important role of BAS in producing HMF via the dehydration step is also supported by the observed highest HMF selectiveness on fructose dehydration ($S_{HMF,45\ min}$ = 76%, Figure 4E). The observed catalytic performance of LAS catalyst and BAS catalyst is in good agreement with the importance of acid site identity for cascade glucose conversion.

With a cascade architectural structure and the presence of spatially separated LAS and BAS, the Al_{ALD}@m-SA gave a much enhanced catalytic performance such that, after 3 h of reaction, *ca.* 93% glucose was converted, and high selectivity to HMF of 66% was achieved (Figure 4C). Additionally, as demonstrated by Table 2, Al_{ALD}@m-SA showed the best

https://doi.org/10.1021/jacsau.3c00396
JACS Au 2023, 3, 2586−2596

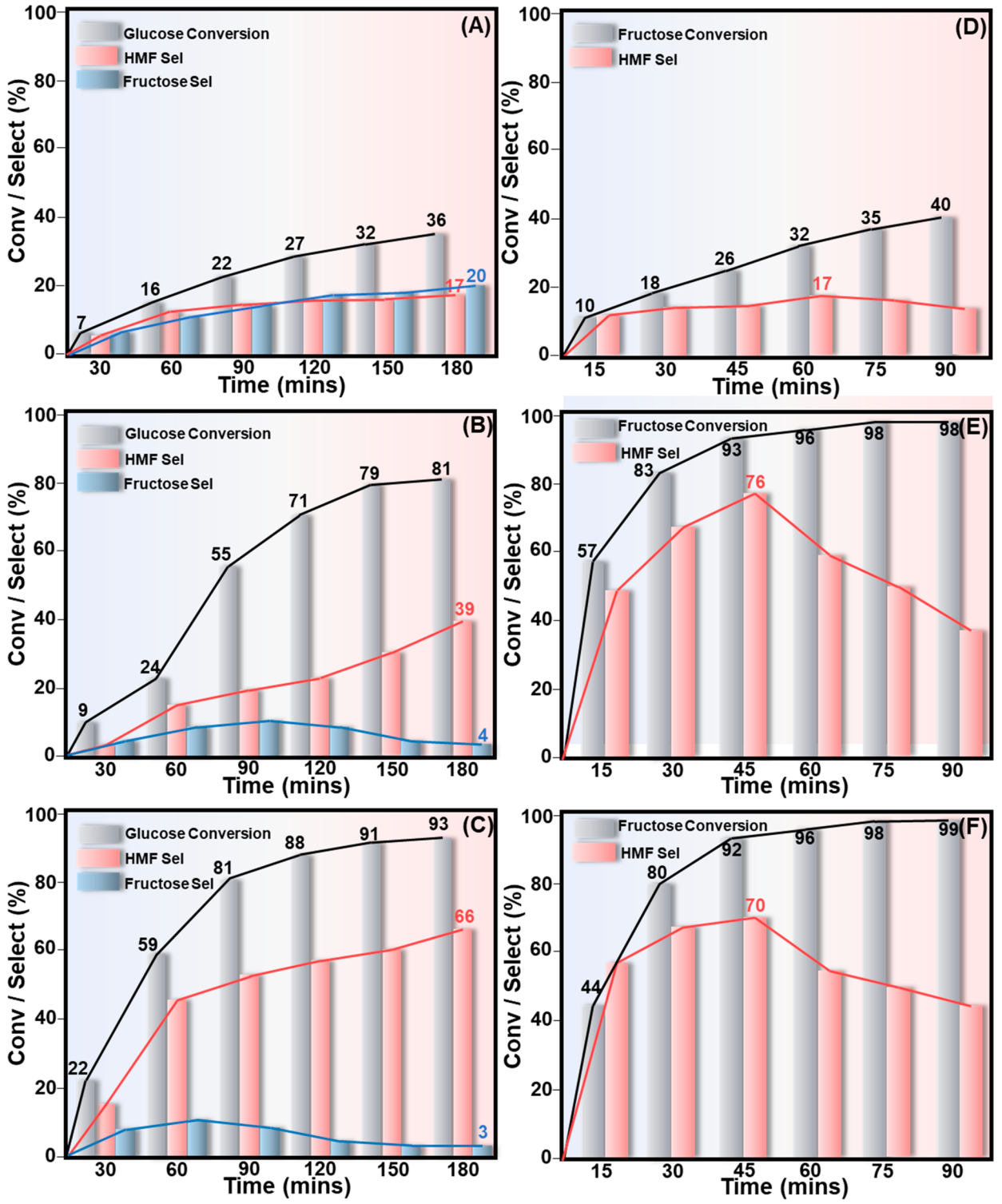

Figure 4. Glucose conversion to HMF with (A) Al_{ALD}@m-S, (B) m-SA, and (C) Al_{ALD}@m-SA catalysts. Fructose dehydration to HMF with (D) Al_{ALD}@m-S, (E) m-SA, and (F) Al_{ALD}@m-SA catalysts. Reaction conditions: 20 mg of Al_{ALD}@high silica substrate catalysts, 2 mL of cosolvent (DMSO/Water = 7/3) containing 60 mg of glucose or fructose at 160 °C under continuous stirring.

catalytic activity regarding the calculation of turnover frequency (TOF). In the first 30 min of the reaction, the high TOF and relatively low HMF selectivity over Al_{ALD}@m-SA can be explained by the high concentration of only LAS on the outermost alumina nanolayer coated by the ALD process. Because the BAS is only present inside the nanopores of the support, the free surface diffusion of reactant directly to BAS is hindered.[16] The limited contact between glucose and/or glucose isomer at the beginning of the reaction leads to the low initial selectivity of HMF. As the cascade glucose conversion reaction progressed, the HMF selectivity increased significantly while the fructose selectivity reduced on Al_{ALD}@m-SA. This is because the fructose produced further diffuses along the catalyst from the outermost surface LAS to BAS inside the

https://doi.org/10.1021/jacsau.3c00396
JACS Au 2023, 3, 2586−2596

Table 2. Summary of Catalytic Data of Glucose Conversion to HMF over the Catalysts

catalysts	$C_{Glucose}$ [a] (%)	S_{HMF} [b] (%)	$S_{Fructose}$ [b] (%)	TOF[c] (h^{-1})
Al_{ALD}@m-SA	59(93)	43(66)	11(3)	6.00
Al_{ALD}@m-S	16(36)	13(17)	10(20)	1.26
m-SA	24(81)	19(39)	9(4)	3.54
m-S	3(21)	12(14)	18(13)	-

[a] $C_{Glucose}$ refers to the conversion of glucose. [b] $S_{HMF}/S_{Fructose}$ refers to the selectivity of 5-hydroxymethylfurfural/fructose. [c] TOF refers to the turnover frequency.

nanopores to produce HMF. It is also supported by the relatively high fructose selectivity at only the first hour of the reaction ($S_{fructose,60\ min}$ = 11%, Figure 4C). Consistently, in fructose dehydration, a relatively slower initial reaction speed on Al_{ALD}@m-SA compared to m-SA with freely accessible Brønsted acidity has been recorded ($C_{fructose,15\ min}$ = 44% and $C_{fructose,15\ min}$ = 57%, respectively. Figure 4E,F). This is because the BAS on Al_{ALD}@m-SA is not distributed on the outermost surface but only distributed inside the nanopores.

Except for the advantage of the control of diffusion from the outermost surface LAS to BAS inside the nanopores, the spatial separation of LAS and BAS limits the synergistic effect, resulting in a more uniform distribution of acidity. It benefits the cascade catalytic performance of the Al_{ALD}@m-SA since side reactions such as overoxidation and rehydration of HMF are preferred on strong BAS and LAS.[43] With the control of diffusion and surface acidity, the cascade-structured LAS-BAS system contributes to the enhanced cascade reaction performance.

Glucose conversion has also been conducted on a powder mixture of BAS catalyst, m-SA, and LAS catalyst, Al_{ALD}@m-S (Figure S8), in order to construct a BAS-LAS system without cascade architectural structure and no diffusion control. Under identical reaction conditions, the reactant should have access to the active sites of the physical mixture of the BAS catalyst and LAS catalyst. Without diffusion control, the observed $C_{Glucose,\ 180\ min}$ = 63% and $S_{HMF,180\ min}$ = 33% are much lower than that of the cascade architectural structured BAS-LAS system, which supports the importance of the spatially well-separated LAS and BAS for cascade reaction catalytic performance improvement. Through the comparison of catalysts with and without a cascade structure, our primary aim was to isolate and analyze the specific influence of the cascade architectural design. Furthermore, the beneficial effect of the BAS-LAS system with a cascade structure was evident from the significant enhancement in HMF selectivity when compared to other amorphous silica−alumina counterparts lacking a spatially separated BAS-LAS system.

Compared to amorphous silica−alumina prepared by typical coprecipitation and sol−gel synthesis without the precise control of acid site location, with close n(Si)/n(Al) ratio (9.0, 9.0, and 7.5 for $ASA_{coprecipitation}$, $ASA_{sol-gel}$, and Al_{ALD}@m-SA, respectively), the prepared Al_{ALD}@m-SA in this study showed more than 9-fold (Al_{ALD}@m-SA 66% vs $ASA_{coprecipitation}$ 6.3%) and 3-fold (Al_{ALD}@m-SA 66% vs $ASA_{sol-gel}$ 18.8%) enhancement in HMF yield at identical conditions.[44] Besides, under comparable reaction conditions, the Al_{ALD}@m-SA with a spatially separated LAS-BAS system showed better performance than the bi-acidic catalysts with disorderly arranged acid sites, such as zeolites of Sn-Beta,[45,46] MCM41,[47] ZSM-5,[48] SBA15,[49] etc. (Table S3).

Additionally, recyclability, an important performance factor for practical applications, has been studied under identical reaction conditions. Figure 5A−C displays the reusability of the catalysts. After recycling, only a slight reduction in glucose conversion was observed for catalysts. These observations support the notion that the ALD-deposited alumina overlayer can stay stable on the outermost surface of the support, which is independent of the stability of the substrate. The slight reduction might originate from the tiny amount of sample loss during the wash and activation processes among cycles.

Based on the characterizations and catalytic performance tests, the structure-acidity-catalytic performance relationship has been plotted (Figure 6). On the ALD-generated overcoat,

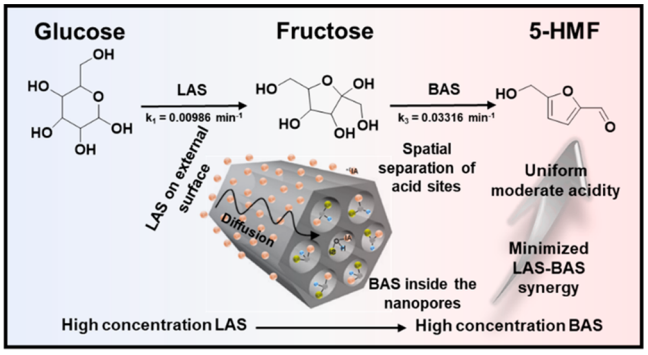

Figure 6. Proposed cascade reaction scheme for glucose conversion into HMF on Al_{ALD}@m-SA.

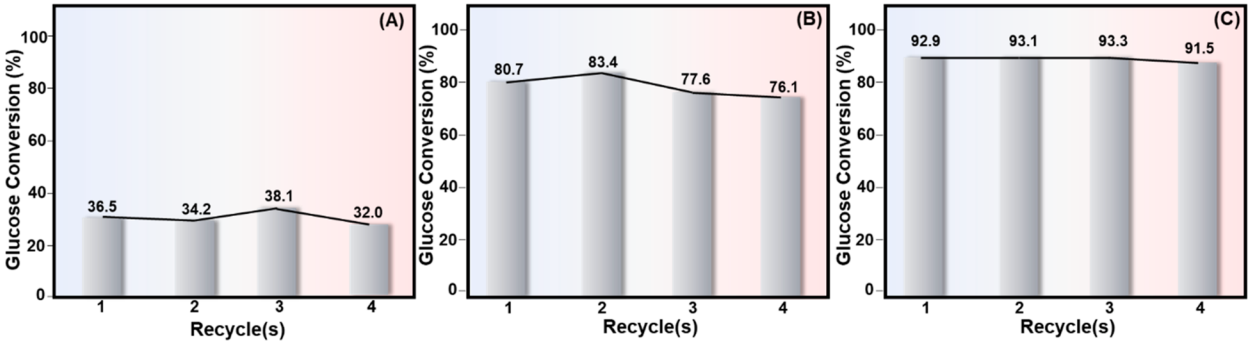

Figure 5. Recycling experiments for glucose conversion with (A) Al_{ALD}@m-S, (B) m-SA, and (C) Al_{ALD}@m-SA catalysts. Reaction conditions: 20 mg of Al_{ALD}@high silica substrate catalysts, 2 mL cosolvent (DMSO/Water = 7/3) containing 60 mg glucose or fructose at 160 °C under continuous stirring.

https://doi.org/10.1021/jacsau.3c00396
JACS Au 2023, 3, 2586−2596

the alumina nanolayer contains LAS with a high concentration on the outermost surface. The concentrated reactant glucose efficiently isomerizes into intermediate fructose on the outermost surface. Because the distribution of BAS is predominantly inside the nanopores of the silica−alumina substrate instead of the alumina overlayer, the physical distance between LAS and BAS limits the surface diffusion of absorbed glucose. This results in the introduced glucose always come into contact with the surface LAS first, followed by the produced isomer, i.e., fructose, coming into contact with the BAS inside the nanopores. The unique geometric distribution of the LAS on the outermost overlayer and the BAS inside the nanopores effectively promote the stepwise diffusion and occurrence of the cascade reaction of glucose isomerization and fructose dehydration.

In conclusion, this work demonstrates the design of a bi-acidic solid acid catalyst with cascade architectural structured BAS and LAS. Via the TEM, EELS visualizations, and 1D and 2D ssNMR methodologies, we successfully demonstrated that the alumina overcoat produced by the ALD process mainly contributes to the formation of LAS on the external surface. With the BAS inside the nanopores of the silica−alumina substrate, the LAS on the outermost surface and BAS inside the nanopores are geometrically separated, thereby leading to the formation of cascade architecturally structured surface acid sites with moderate and uniform acidity. We also demonstrated that with directional diffusion of glucose reactant from the LAS domain to the BAS domain, excellent catalytic performances on both glucose conversion and HMF selectivity have been observed over the Al_{ALD}@m-SA. The superior catalytic performance of the cascade structured Al_{ALD}@m-SA, compared to its counterparts without the cascade architectural structure, including $ASA_{sol-gel}$, $ASA_{nanodomain}$, and previously published zeolites such as ZSM-5, zeolite H, and SBA-15 (refer to Table S3), highlights the significance of the cascade architectural structure in enhancing the cascade reaction performance. This observation reinforces the potential of the cascade design for optimizing catalytic processes. Thus, this work paves the way for designing a bi-acidic catalyst with a unique cascade architectural structure for efficient cascade reactions.

MATERIALS AND METHODS

Catalyst Preparation

The construction of the mesostructured amorphous silica substrate was reported previously by our group via a one-step room-temperature preparation.[24] Utilized chemicals were purchased from Sigma-Aldrich and are listed here: ammonium hydroxide solution (28% NH_3 in H_2O, 0.9 g/mL), tetraethylorthosilicate (TEOS, >98%), hexadecyltrimethylammonium chloride solution (CTAC, 25 wt % in H_2O), and aluminum(III) nitrate nonahydrate ($Al(NO_3)_3{\cdot}9H_2O$, >98%). Briefly, without aluminum precursor loading, the pure silica was synthesized as follows: in 200 mL of deionized water with 5 mL of CTAC and 5 mL of NH_4OH solution, 5 mL of TEOS was added under vigorous stirring at a temperature of 298 K. After the formation of white colored gel, the formed gel underwent 20 min of ultrasonication, followed by another 1 h of vigorous stirring. The solid content of the prepared gel was then collected via vacuum filtration and washed with deionized water and ethanol three times. After drying the obtained solid overnight under 80 °C, the collected solid experienced a calcination process at 550 °C for 6 h with a temperature increase rate of 1 °C/min from room temperature under the presence of air. The prepared substrate is named m-S (mesostructured amorphous silica). Compared to the preparation for pure m-S, for alumina doped m-S, the only difference in the preparation method is the addition of $Al(NO_3)_3{\cdot}9H_2O$ after the formation of white gel. With the molar ratio of $n(Si)/n(Al) = 40$, the prepared catalyst is named m-SA (mesostructured amorphous silica−alumina).

Al_2O_{3ALD} on prepared substrate (Al_{ALD}@high silica substrate) was performed by a custom-made rotary fluidized ALD reactor (AngstromBlock Scale-R01 ALD system) as reported in a previous study.[50] The temperature of the reactor was set at 200 °C and the rotation speed of the powder cartridge was set to 100 rpm. The Al precursor was trimethylaluminum (TMA) and oxygen source was deionized H_2O. The pulse time and purge time for both TMA and H_2O were 60 and 120 s, respectively. Twenty cycles of Al_2O_3 ALD were carried out on samples in this work, and after 500 °C calcination for 6 h, the catalysts were named Al_{ALD}@m-S and Al_{ALD}@m-SA.

Chemical and Physical Properties Characterization

Wide-angle XRD patterns were recorded from fine powder samples by using a PANalytical XPert Pro powder diffractometer in the Bragg−Brentano geometry with Co Kα radiation (λ = 0.1789 nm, 40 kV, 40 mA). The nitrogen adsorption−desorption isotherms were measured via an Autosorb IQ-C system. The system was cooled to 77 K prior to the experiment to avoid chemisorption by liquid nitrogen. The specific surface area and the mesopore properties were calculated via the Brunauer−Emmett−Teller (BET) method and the Barrett−Joyner−Halenda (BJT) method, respectively. The morphology of the catalysts was characterized by high-resolution transmission electron microscopy (HRTEM) over FEI Themis Z with a double spherical aberration corrector operated on 300 keV. The electron energy loss spectroscopy (EELS) mapping is acquired over the same instrument with a Gatan electron prism. The surface chemical analysis of the catalysts was measured by a Thermo Fisher ESCALAB 250Xi spectrometer with a focused monochromatic Al Kα-rays (1486.6 eV) source. The surveys of X-ray photoelectron spectroscopy (XPS) measurements have been applied to measure the surface compositions with a passing energy of 20 eV.

The solid-state NMR spectra were recorded at 11.7 T on a Bruker Avance III 500WB spectrometer at room temperature. Using 4 mm ZrO_2 rotors, one-dimensional (1D) single pulse (SP) excitation of ^1H and ^{31}P spectra were recorded at the resonance frequencies of 500.1 and 202.5 MHz, respectively, using $\pi/2$ excitation pulses. The quantitative ^{31}P MAS NMR measurements were conducted using ammonium dihydrogen phosphate (ADP, >98%, Sigma-Aldrich) as the external standard. The 1D SP excitation of ^{27}Al was acquired at the resonance frequency of 130.3 MHz within 2.5 mm ZrO_2 rotors using a $\pi/6$ excitation pulse. For the measurement of dehydrated samples, the sample was pretreated under 673 K overnight under a nitrogen environment and then sealed into the rotor within a N_2 glovebox, while for hydrated samples, they were exposed to the atmosphere for a week for full hydration prior to the NMR experiments. The $^1H/^{27}Al$ TRAPDOR NMR spectra were obtained via the subtraction of the 200 W ^{27}Al dephasing pulse ^1H spectrum from the ^1H spectrum obtained without this pulse. The two-dimensional (2D) ^{27}Al multiple quantum (MQ) NMR spectra were recorded using the published three-pulse z-filter MQ MAS pulse sequence under MAS rate of 25 kHz.[51] The NMR spectra were simulated based on the Gaussian−Lorentzian peak shapes using Dmfit software.[52]

Catalytic Performance Measurement

In a 25 mL glass pressure reactor, a biphasic system with volume ratio of V(deionized water)/V(dimethyl sulfoxide, DMSO, ≥99.5%, Sigma-Aldrich) = 3/7 has been prepared as the solvent. Reactant 60 mg of glucose (≥99.5%, Sigma-Aldrich) or D-(−)-fructose (≥99%, Sigma-Aldrich) was then dissolved in the solvent and ready for further catalytic test. Prior to the reaction, the catalysts were pretreated and activated at 673 K under a nitrogen environment, and then 20 mg of catalyst was transferred into the reactor for each run. In an oil bath with a temperature of 433 K, the reaction was conducted with vigorous magnetic stirring. To measure the catalytic performance of catalysts, samples of reaction mixture have been collected every 30 min up to 180 min (for glucose conversion) or every 15 min up to 90

https://doi.org/10.1021/jacsau.3c00396
JACS Au 2023, 3, 2586−2596

min (for fructose conversion). The collected samples were diluted into deionized water and filtered by a 0.22 μm syringe filter for further high-performance liquid chromatography (HPLC) analysis. With mobile phase of filtered 0.005 M H_2SO_4 aqueous solution, the reactant and product were analyzed by an Agilent 1260 system equipped with a Biorad Aminex HPX-87H column (300 × 7.8 mm, 9 μm) and via a refractive index detector and a multiwavelength detector, respectively.

■ ASSOCIATED CONTENT

Supporting Information

The Supporting Information is available free of charge at https://pubs.acs.org/doi/10.1021/jacsau.3c00396.

Supplementary Text including Figures S1−S9, Tables S1−S4, and associated refs (PDF)

■ AUTHOR INFORMATION

Corresponding Authors

Rong Chen − *State Key Laboratory of Intelligent Manufacturing Equipment and Technology, School of Mechanical Science and Engineering, Huazhong University of Science and Technology, Wuhan, Hubei 430074, PR China;* orcid.org/0000-0001-7371-1338; Email: rongchen@mail.hust.edu.cn

Jun Huang − *Laboratory for Catalysis Engineering, School of Chemical and Biomolecular Engineering, Sydney Nano Institute, The University of Sydney, Sydney, NSW 2006, Australia;* orcid.org/0000-0001-8704-605X; Email: jun.huang@sydney.edu.au

Authors

Wenjie Yang − *Laboratory for Catalysis Engineering, School of Chemical and Biomolecular Engineering, Sydney Nano Institute, The University of Sydney, Sydney, NSW 2006, Australia; Department of Engineering, Macquarie University, Sydney, NSW 2019, Australia;* orcid.org/0000-0002-1013-2678

Xiao Liu − *State Key Laboratory of Intelligent Manufacturing Equipment and Technology, School of Mechanical Science and Engineering, Huazhong University of Science and Technology, Wuhan, Hubei 430074, PR China*

Luke A. O'Dell − *Institute for Frontier Materials, Deakin University, Geelong, VIC 3220, Australia;* orcid.org/0000-0002-7760-5417

Xingxu Liu − *Laboratory for Catalysis Engineering, School of Chemical and Biomolecular Engineering, Sydney Nano Institute, The University of Sydney, Sydney, NSW 2006, Australia*

Lizhuo Wang − *Laboratory for Catalysis Engineering, School of Chemical and Biomolecular Engineering, Sydney Nano Institute, The University of Sydney, Sydney, NSW 2006, Australia*

Wenwen Zhang − *Department of Engineering, Macquarie University, Sydney, NSW 2019, Australia*

Bin Shan − *State Key Laboratory of Materials Processing and Die and Mould Technology, School of Materials Science and Engineering, Huazhong University of Science and Technology, Wuhan, Hubei 430074, PR China*

Yijiao Jiang − *Department of Engineering, Macquarie University, Sydney, NSW 2019, Australia;* orcid.org/0000-0002-6191-9825

Complete contact information is available at: https://pubs.acs.org/10.1021/jacsau.3c00396

Author Contributions

Conceptualization: JH, RC, BS. Methodology: WY, XL, LD. Investigation: WY, XXL, LW. Visualization: WY. Supervision: JH, YJ, RC. Writing—original draft: WY. Writing—review and editing: JH, YJ, RC, BS. CRediT: **Wenjie Yang** data curation, formal analysis, investigation, writing-original draft, writing-review & editing; **Xiao Liu** investigation, resources; **Luke A. O'Dell** conceptualization, funding acquisition, investigation, methodology, resources, validation, writing-review & editing; **Xingxu Liu** investigation; **Lizhuo Wang** investigation; **Wenwen Zhang** investigation; **Bin Shan** conceptualization, methodology, project administration; **Yijiao Jiang** funding acquisition, project administration, supervision; **Rong Chen** conceptualization, funding acquisition, project administration, resources, supervision, writing-review & editing; **Jun Huang** conceptualization, funding acquisition, methodology, project administration, resources, supervision, validation, writing-review & editing.

Funding

The Australian Research Council Discovery Project (DP220102851) ARC Future Fellowships (FT220100601) the National Natural Science Foundation of China (51835005) HUST (Grant No. DMETKF2020010).

Notes

The authors declare no competing financial interest.

■ ACKNOWLEDGMENTS

Authors acknowledge the State Key Laboratory of Digital Manufacturing Equipment and Technology, the facilities of Sydney Analytical, a core research facility at the University of Sydney, and NMR facility of Deakin University. W.Y. acknowledge the support of the University of Sydney International Scholarship Strategic (USydIS-Strategic).

■ REFERENCES

(1) Busca, G. Silica-alumina catalytic materials: A critical review. *Catal. Today* **2020**, *357*, 621−629.

(2) Marianou, A. A.; Michailof, C. M.; Pineda, A.; Iliopoulou, E.; Triantafyllidis, K.; Lappas, A. Effect of Lewis and Brønsted acidity on glucose conversion to 5-HMF and lactic acid in aqueous and organic media. *Appl. Catal. A: General* **2018**, *555*, 75−87.

(3) Otomo, R.; Yokoi, T.; Kondo, J. N.; Tatsumi, T. Dealuminated Beta zeolite as effective bifunctional catalyst for direct transformation of glucose to 5-hydroxymethylfurfural. *Appl. Catal. A: General* **2014**, *470*, 318−326.

(4) Sandoval-Díaz, L.-E.; González-Amaya, J.-A.; Trujillo, C.-A. General aspects of zeolite acidity characterization. *Microporous and mesoporous materials* **2015**, *215*, 229−243.

(5) Coster, D.; Blumenfeld, A.; Fripiat, J. Lewis acid sites and surface aluminum in aluminas and zeolites: a high-resolution NMR study. *J. Phys. Chem.* **1994**, *98* (24), 6201−6211.

(6) Chu, Y.; Yi, X.; Li, C.; Sun, X.; Zheng, A. Brønsted/Lewis acid sites synergistically promote the initial C-C bond formation in the MTO reaction. *Chemical science* **2018**, *9* (31), 6470−6479.

(7) Xin, S.; Wang, Q.; Xu, J.; Chu, Y.; Wang, P.; Feng, N.; Qi, G.; Trébosc, J.; Lafon, O.; Fan, W. The acidic nature of "NMR-invisible" tri-coordinated framework aluminum species in zeolites. *Chemical science* **2019**, *10* (43), 10159−10169.

(8) Wang, Z.; O'Dell, L. A.; Zeng, X.; Liu, C.; Zhao, S.; Zhang, W.; Gaborieau, M.; Jiang, Y.; Huang, J. Insight into Three-Coordinate Aluminum Species on Ethanol-to-Olefin Conversion over ZSM-5 Zeolites. *Angew. Chem., Int. Ed.* **2019**, *58* (50), 18061−18068.

(9) Zhao, S.; Yang, W.; Kim, K. D.; Wang, L.; Wang, Z.; Ryoo, R.; Huang, J. Synergy of Extraframework Al^{3+} Cations and Brønsted Acid Sites on Hierarchical ZSM-5 Zeolites for Butanol-to-Olefin Conversion. *J. Phys. Chem. C* **2021**, *125* (21), 11665−11676.
(10) Dijkmans, J.; Dusselier, M.; Gabriëls, D.; Houthoofd, K.; Magusin, P. C.; Huang, S.; Pontikes, Y.; Trekels, M.; Vantomme, A.; Giebeler, L. Cooperative catalysis for multistep biomass conversion with Sn/Al Beta zeolite. *ACS Catal.* **2015**, *5* (2), 928−940.
(11) Li, G.; Gao, L.; Sheng, Z.; Zhan, Y.; Zhang, C.; Ju, J.; Zhang, Y.; Tang, Y. A Zr-Al-Beta zeolite with open Zr (iv) sites: an efficient bifunctional Lewis-Brønsted acid catalyst for a cascade reaction. *Catalysis Science & Technology* **2019**, *9* (15), 4055−4065.
(12) Qi, G.; Wang, Q.; Xu, J.; Trébosc, J.; Lafon, O.; Wang, C.; Amoureux, J. P.; Deng, F. Synergic Effect of Active Sites in Zinc-Modified ZSM-5 Zeolites as Revealed by High-Field Solid-State NMR Spectroscopy. *Angew. Chem., Int. Ed.* **2016**, *128* (51), 16058−16062.
(13) Gao, P.; Wang, Q.; Xu, J.; Qi, G.; Wang, C.; Zhou, X.; Zhao, X.; Feng, N.; Liu, X.; Deng, F. Brønsted/Lewis acid synergy in methanol-to-aromatics conversion on Ga-modified ZSM-5 zeolites, as studied by solid-state NMR spectroscopy. *ACS Catal.* **2018**, *8* (1), 69−74.
(14) Huang, J.; Jiang, Y.; Marthala, V. R.; Thomas, B.; Romanova, E.; Hunger, M. Characterization and acidic properties of aluminum-exchanged zeolites X and Y. *J. Phys. Chem. C* **2008**, *112* (10), 3811−3818.
(15) An, H.; Kweon, S.; Kang, D.-C.; Shin, C.-H.; Kim, J. F.; Park, M. B.; Min, H.-K. Cascade conversion of glucose to 5-hydroxymethylfurfural over Brönsted-Lewis bi-acidic SnAl-beta zeolites. *Korean Journal of Chemical Engineering* **2021**, *38* (6), 1161−1169.
(16) Wang, Z.; Buechel, R.; Jiang, Y.; Wang, L.; Xu, H.; Castignolles, P.; Gaborieau, M.; Lafon, O.; Amoureux, J.-P.; Hunger, M. Engineering the distinct structure interface of subnano-alumina domains on silica for acidic amorphous silica-alumina toward biorefining. *JACS Au* **2021**, *1* (3), 262−271.
(17) Le, T.; Qin, W.; Agarwal, A.; Nikolopoulos, N.; Fu, D.; Patton, M.; Weiland, C.; Bare, S.; Palmer, J.; Weckhuysen, B.; Rimer, J. Elemental zoning enhances mass transport in zeolite catalysts for methanol to hydrocarbons. *Nature Catalysis* **2023**, *6*, 254−265.
(18) Cao, K.; Cai, J.; Liu, X.; Chen, R. Catalysts design and synthesis via selective atomic layer deposition. *Journal of Vacuum Science Technology A: Vacuum, Surfaces, Films* **2018**, *36* (1), 010801.
(19) Mouat, A. R.; George, C.; Kobayashi, T.; Pruski, M.; Van Duyne, R. P.; Marks, T. J.; Stair, P. C. Highly dispersed $SiOx/Al_2O_3$ catalysts illuminate the reactivity of isolated silanol sites. *Angew. Chem., Int. Ed.* **2015**, *127* (45), 13544−13549.
(20) Ardagh, M. A.; Bo, Z.; Nauert, S. L.; Notestein, J. M. Depositing SiO_2 on Al_2O_3: A route to tunable Brønsted acid catalysts. *ACS Catal.* **2016**, *6* (9), 6156−6164.
(21) Krishna, S. H.; Zhang, L.; Hermans, I.; Huber, G. W.; Kuech, T. F.; Dumesic, J. A. Rates of levoglucosanol hydrogenolysis over Brønsted and Lewis acid sites on platinum silica-alumina catalysts synthesized by atomic layer deposition. *Journal of catalysis* **2020**, *389*, 111−120.
(22) Zhu, L.; Fu, X.; Hu, Y.; Hu, C. Controlling the Reaction Networks for Efficient Conversion of Glucose into 5-Hydroxymethylfurfural. *ChemSusChem* **2020**, *13* (18), 4812−4832.
(23) Meng, Y.; Yang, S.; Li, H. Electro-and Photocatalytic Oxidative Upgrading of Bio-based 5-Hydroxymethylfurfural. *ChemSusChem* **2022**, *15* (13), No. e202102581.
(24) Wang, Z.; Jiang, Y.; Rachwalik, R.; Liu, Z.; Shi, J.; Hunger, M.; Huang, J. One-Step Room-Temperature Synthesis of [Al] MCM-41 Materials for the Catalytic Conversion of Phenylglyoxal to Ethyl-mandelate. *ChemCatChem.* **2013**, *5* (12), 3889−3896.
(25) Zhang, W.; Zhu, Y.; Xu, H.; Gaborieau, M.; Huang, J.; Jiang, Y. Glucose conversion to 5-hydroxymethylfurfural on zirconia: tuning surface sites by calcination temperatures. *Catal. Today* **2020**, *351*, 133−140.
(26) Kaushik, M.; Leroy, C.; Chen, Z.; Gajan, D.; Willinger, E.; Müller, C. R.; Fayon, F.; Massiot, D.; Fedorov, A.; Copéret, C. Atomic-scale structure and its impact on chemical properties of aluminum oxide layers prepared by atomic layer deposition on silica. *Chem. Mater.* **2021**, *33* (9), 3335−3348.
(27) Hakim, L.; Blackson, J.; Weimer, A. Modification of interparticle forces for nanoparticles using atomic layer deposition. *Chem. Eng. Sci.* **2007**, *62* (22), 6199−6211.
(28) Liang, X.; Weimer, A. W. Photoactivity passivation of TiO_2 nanoparticles using molecular layer deposited (MLD) polymer films. *J. Nanopart. Res.* **2010**, *12*, 135−142.
(29) Du, H.; Chen, S.; Wang, H.; Lu, J. Acidic alumina overcoating on platinum nanoparticles: Close metal-acid proximity enhances bifunctionality for glycerol hydrogenolysis. *Chinese Journal of Catalysis* **2017**, *38* (7), 1237−1244.
(30) Kriesel, J. W.; Sander, M. S.; Tilley, T. D. General route to homogeneous, mesoporous, multicomponent oxides based on the thermolytic transformation of molecular precursors in non-polar media. *Adv. Mater.* **2001**, *13* (5), 331−335.
(31) Yang, W.; Kim, K. D.; O'Dell, L. A.; Wang, L.; Xu, H.; Ruan, M.; Wang, W.; Ryoo, R.; Jiang, Y.; Huang, J. Brønsted acid sites formation through penta-coordinated aluminum species on alumina-boria for phenylglyoxal conversion. *J. Catal.* **2022**, *416*, 375−386.
(32) Xu, S.; Jaegers, N. R.; Hu, W.; Kwak, J. H.; Bao, X.; Sun, J.; Wang, Y.; Hu, J. Z. High-field one-dimensional and two-dimensional ^{27}Al magic-angle spinning nuclear magnetic resonance study of θ-, δ-, and γ-Al_2O_3 dominated aluminum oxides: toward understanding the Al sites in γ-Al2O3. *ACS omega* **2021**, *6* (5), 4090−4099.
(33) Khivantsev, K.; Jaegers, N. R.; Kwak, J. H.; Szanyi, J.; Kovarik, L. Precise Identification and Characterization of Catalytically Active Sites on the Surface of γ-Alumina. *Angew. Chem., Int. Ed.* **2021**, *133* (32), 17663−17671.
(34) Zheng, A.; Liu, S.-B.; Deng, F. Acidity characterization of heterogeneous catalysts by solid-state NMR spectroscopy using probe molecules. *Solid State Nucl. Magn. Reson.* **2013**, *55*, 12−27.
(35) Rakiewicz, E. F.; Peters, A. W.; Wormsbecher, R. F.; Sutovich, K. J.; Mueller, K. T. Characterization of acid sites in zeolitic and other inorganic systems using solid-state ^{31}P NMR of the probe molecule trimethylphosphine oxide. *J. Phys. Chem. B* **1998**, *102* (16), 2890−2896.
(36) Obenaus, U.; Dyballa, M.; Lang, S.; Scheibe, M.; Hunger, M. Generation and properties of Brønsted acid sites in bifunctional Rh-, Ir-, Pd-, and Pt-containing zeolites Y investigated by solid-state NMR spectroscopy. *J. Phys. Chem. C* **2015**, *119* (27), 15254−15262.
(37) Yang, W.; Wang, Z.; Huang, J.; Jiang, Y. Qualitative and quantitative analysis of acid properties for solid acids by solid-state nuclear magnetic resonance spectroscopy. *J. Phys. Chem. C* **2021**, *125* (19), 10179−10197.
(38) Yu, I. K.M.; Tsang, D. C.W. Conversion of biomass to hydroxymethylfurfural: A review of catalytic systems and underlying mechanisms. *Bioresource technology* **2017**, *238*, 716−732.
(39) Ordomsky, V.; Sushkevich, V.; Schouten, J.; Van Der Schaaf, J.; Nijhuis, T. Glucose dehydration to 5-hydroxymethylfurfural over phosphate catalysts. *Journal of catalysis* **2013**, *300*, 37−46.
(40) Moreno-Recio, M.; Santamaría-González, J.; Maireles-Torres, P. Brönsted and Lewis acid ZSM-5 zeolites for the catalytic dehydration of glucose into 5-hydroxymethylfurfural. *Chem. Eng. J.* **2016**, *303*, 22−30.
(41) Kim, Y.; Mittal, A.; Robichaud, D.; Pilath, H.; Etz, B.; John, P.; Johnson, D.; Seonah, K. Prediction of hydroxymethylfurfural yield in glucose conversion through investigation of Lewis acid and organic solvent effects. *ACS Catal.* **2020**, *10* (24), 14707−14721.
(42) Jimenez-Morales, I.; Moreno-Recio, M.; Santamaria-Gonzalez, J.; Maireles-Torres, P.; Jimenez-Lopez, A. Production of 5-hydroxymethylfurfural from glucose using aluminium doped MCM-41 silica as acid catalyst. *Appl. Catal. B: Environmental* **2015**, *164*, 70−76.
(43) Ordomsky, V.; Sushkevich, V.; Schouten, J.; Van Der Schaaf, J.; Nijhuis, T. Glucose dehydration to 5-hydroxymethylfurfural over phosphate catalysts. *Journal of catalysis* **2013**, *300*, 37−46.

https://doi.org/10.1021/jacsau.3c00396
JACS Au 2023, 3, 2586−2596

(44) Wang, Z.; Li, T.; Jiang, Y.; Lafon, O.; Liu, Z.; Trébosc, J.; Baiker, A.; Amoureux, J.-P.; Huang, J. Acidity enhancement through synergy of penta-and tetra-coordinated aluminum species in amorphous silica networks. *Nat. Commun.* **2020**, *11* (1), 225.
(45) Oozeerally, R.; Pillier, J.; Kilic, E.; Thompson, P. B.; Walker, M.; Griffith, B. E.; Hanna, J. V.; Degirmenci, V. J. Gallium and tin exchanged Y zeolites for glucose isomerisation and 5-hydroxymethyl furfural production. *Appl. Catal. A: General* **2020**, *605*, 117798.
(46) Saenluang, K.; Thivasasith, A.; Dugkhuntod, P.; Pornsetmetakul, P.; Salakhum, S.; Namuangruk, S.; Wattanakit, C. In situ synthesis of Sn-beta zeolite nanocrystals for glucose to hydroxymethylfurfural (HMF). *Catalysts* **2020**, *10* (11), 1249.
(47) Jiménez-Morales, I.; Santamaría-González, J.; Jiménez-López, A.; Maireles-Torres, P. Glucose dehydration to 5-hydroxymethylfurfural on zirconium containing mesoporous MCM-41 silica catalysts. *Fuel* **2014**, *118*, 265−271.
(48) Chung, N. H.; Oanh, V. T.; Thoa, L. K.; Hoang, P. Catalytic conversion of glucose into 5-hydroxymethyl furfural over Cu-Cr/ZSM-5 zeolite. *Waste and biomass valorization* **2020**, *150* (1), 170−177.
(49) Peng, K.; Li, X.; Liu, X.; Wang, Y. Hydrothermally stable Nb-SBA-15 catalysts applied in carbohydrate conversion to 5-hydroxymethyl furfural. *Molecular Catalysis* **2017**, *441*, 72−80.
(50) Duan, C.-L.; Liu, X.; Shan, B.; Chen, R. Fluidized bed coupled rotary reactor for nanoparticles coating via atomic layer deposition. *Rev. Sci. Instrum.* **2015**, *86* (7), 075101.
(51) Amoureux, J.-P.; Fernandez, C.; Steuernagel, S. ZFiltering in MQMAS NMR. *J. Magn. Reson.* **1996**, *123* (1), 116−118.
(52) Massiot, D.; Fayon, F.; Capron, M.; King, I.; Le Calvé, S.; Alonso, B.; Durand, J. O.; Bujoli, B.; Gan, Z.; Hoatson, G. Modelling one-and two-dimensional solid-state NMR spectra. *Magnetic resonance in chemistry* **2002**, *40* (1), 70−76.

https://doi.org/10.1021/jacsau.3c00396
JACS Au 2023, 3, 2586−2596